ADVANCED MATERIALS TECHNOLOGIES
www.advmattechnol.de

Temporary Tattoo pH Sensor with pH-Responsive Hydrogel via Initiated Chemical Vapor Deposition

Katrin Unger, Francesco Greco, and Anna Maria Coclite*

In the expanding field of physiological pH skin sensors, thin temporary tattoo-based devices have gained attention because of ultra-conformal adhesion while providing excellent water vapor transmission. Here, a pH sensor tattoo made of temporary tattoo paper, screen-printed poly(3,4-ethylenedioxythiophene):polystyrene sulfonate electrodes, and pH-responsive hydrogel deposited via initiated chemical vapor deposition, is proposed. The tattoo sensor is easily transferred on skin, maintaining full functionality, and shows excellent conformability to topographical features of epidermis. The investigation of the morphology of all layers within the sensor verifies full control of the desired width of electrodes, thickness of hydrogel, and deposition shielded areas. The hydrogel layer exhibits a reversible pH-responsive swelling of 24.7 ± 0.3% to 38 ± 1%, with respect to the dry state, at pH 4 to pH 6, respectively. Impedance spectroscopy identifies the phase shift at 10 and 1000 Hz as an excellent pH-related property of the sensor, which can be only ascribed to the presence of the hydrogel. The sensors ability to be operated with non-sophisticated read-out hardware and software is also demonstrated.

1. Introduction

Wearable flexible body sensors for in situ physiological measurements have become of major interest in healthcare because of the possibility to monitor permanently the patients state of health, providing the chance to prematurely detect deterioration and act at early stage of diseases.[1–7] Body fluids such as sweat, saliva, or tears contain various chemical substances that provide insight about the state of health.[8–10] Sweat is of particular interest as it is accessible via the body surface, readily available, and its composition can be directly linked to that of blood.[11–14] Sweat is a complex mixture of several ion species, ammonium, glucose, and lactate among others and provides rich source of information about the physiological state of the body.

K. Unger, F. Greco, A. M. Coclite
Institute of Solid State Physics
Graz University of Technology
Petersgasse 16, Graz 8010, Austria
E-mail: katrin.unger@tugraz.at

The ORCID identification number(s) for the author(s) of this article can be found under https://doi.org/10.1002/admt.202100717.

DOI: 10.1002/admt.202100717

The pH of eccrine sweat is slightly acid with a pH value in the range from 4.5 to 7 forming together with sebum the acid mantel of the skin, which acts as a natural barrier against bacteria, viral infections, and other contaminants that might penetrate the skin. The combination of the acid skin with the alkaline blood equips the body with a great defense against bacteria pathogens. Different exogenous (skin disease, hormones, electrolyte loss) or endogenous (alkaline cosmetics, drugs) factors can disrupt the epidermal pH, leading to a dehydrated, broken, and vulnerable skin.[15–17] Skin-worn pH sensors were already successfully implemented in patches,[14,18–20] wristbands,[13,21,22] textiles,[23,24] or temporary tattoos.[25,26] Typical detection strategies imply optical (colorimetric)[27,28] and electroanalytical (potentiometric)[29,30] techniques (detection methods of sweat sensors are listed in Table S1, Supporting Information). While optical pH skin sensors have the benefits of a visible read-out and do not require a power supply, only with electroanalytical methods continuous tracking is possible.

When analyzing human sweat in real-time, certain challenges need to be addressed, such as little sample production, large variety of analytes, or the evaporation of old sweat. For that reason, in 2012 the first tattoo-based electrochemical sensor for skin-contact application was proposed by the group of Wang et al. by screen-printing working, reference, and counter electrodes on top of a market available temporary tattoo paper.[31] Selectivity of the sensor could be adjusted by functionalization of the working electrode or by supplementary electrodes.[32–36]

Due to their thinness (< 1 µm thickness), tattoo sensors have the great benefit of smoothly follow the grooves and ridges of the skin topography—just as a second skin—while providing excellent water vapor transport properties, letting the skin "breath."[37–39] The combination of maximizing the sensor/skin actual contact area and the removal of perspiration is highly needed. Indeed average sweat production in an adult is in the range of 1–20 µL min^{-1} mm^{-2} at rest, but it rises several orders of magnitude during exercise.[10,40] The elaborated tattoo sensors were already tested on human body during exercise, verifying accurate measurements and instantaneous response toward the pH. On the contrary, the manufacturing process required transfer of stand-alone thin films, and the challenge of measuring little sample amounts is not solved to satisfaction. Typical sweat glands are spread on human skin with a distance of 1 mm. To distribute the analyte on the complete sensor surface, new materials need to be explored.

Solution-based methods, such as screen- or inkjet-printing are attractive fabrication processes, because they are performed under ambient condition and are easily scalable. Nevertheless, in combination with tattoo substrates these methods are mostly limited to water-based inks as otherwise the tattoo layers integrity and/or transferability get compromised.[41]

Widening the possible manufacturing methods and materials, recently also vacuum-based deposition techniques have been utilized to functionalize transferable tattoos.[25] Techniques that necessitate high or ultrahigh vacuum are costly, and time-consuming especially when thinking of the tattoo paper as substrate which is typically water-affine, and has a large surface area. On the contrary, initiated chemical vapor deposition (iCVD) is a low-vacuum (<100 mTorr) and scalable technique that synthesize thin and conformal polymer coatings with high retention of functional groups on various substrates at low temperatures (20–60 °C).[42–44] An initiator species is added to the monomer in the vacuum chamber feed. The initiator has a labile bond that decomposes at relatively hot filament (≈280 °C), producing radicals, which start the polymerization at the surface, where the monomer is adsorbed. At such temperatures, the monomer is not fragmented and retains its structure.[45,46] With this technique, delicate substrates such as tissue paper,[47,48] pharmaceutics,[49,50] or even ionic liquids[51,52] were already successfully coated.

An interesting branch of functional polymers achievable by iCVD is that of responsive hydrogels that absorb water depending on a certain stimulus.[53] The rich variations of the responsiveness that can be accessed via iCVD were already demonstrated for humidity,[54,55] temperature,[56,57] light,[58,59] and pH.[60,61] pH-responsive hydrogels comprise weak acidic (or basic) functional groups which can be ionized depending on the pH level. pH-responsive hydrogels were already used as detection materials in pH sensors with the disadvantage of reacting also to the ionic strength, which leads to a nonselective response.

The swelling of the hydrogel versus the pH exhibits a first-order phase transition with a material characteristic apparent dissociation constant p$K\alpha$. Above p$K\alpha$, the acidic functional groups deprotonate and repel each other, resulting in a swelling of the polymer network. Below p$K\alpha$, the acid units can form strong hydrogen bonds among themselves and the polymer chain collapses. Not only the swelling changes drastically but also the dielectric properties within the hydrogel exhibit a drastic change at p$K\alpha$. In terms of measuring the pH of the skin (4.5–7), hydrogels made of poly-methacrylic-acid (pMAA) seem promising candidates, as the apparent dissociation constant p$K\alpha$ is about 4.8. pMAA is biocompatible and was already successfully synthesized via iCVD to obtain pharmaceutical drug coatings[50] for pH-dependent release properties.[61,62]

Responsive hydrogels deposited via iCVD enable a complete new sensing material and measurement strategy for sweat sensors, with the great benefit of having a sensing material that soaks up also little amount of sweat, a scalable fabrication process, and an access to an ultrathin all polymer-based environmental-friendly sensor.

Within this study, tattoo-based substrates were screen printed with poly(3,4-ethylenedioxythiophene):polystyrene sulfonate (PEDOT:PSS) electrodes, and further conformally coated with a pH-responsive hydrogel of pMAA via iCVD (**Figure 1**) to achieve an all-polymer pH skin sensor. The fabricated pH sensor tattoo is thoroughly investigated in terms of applicability, morphology, and pH responsiveness concerning swelling and dielectric properties.

2. pH Sensor Tattoo Structure

The temporary tattoo paper used in this study consists of a paper carrier sheet, a water soluble starch layer, and an ethylcellulose (EC) layer (see cross-section within Figure 1), which was

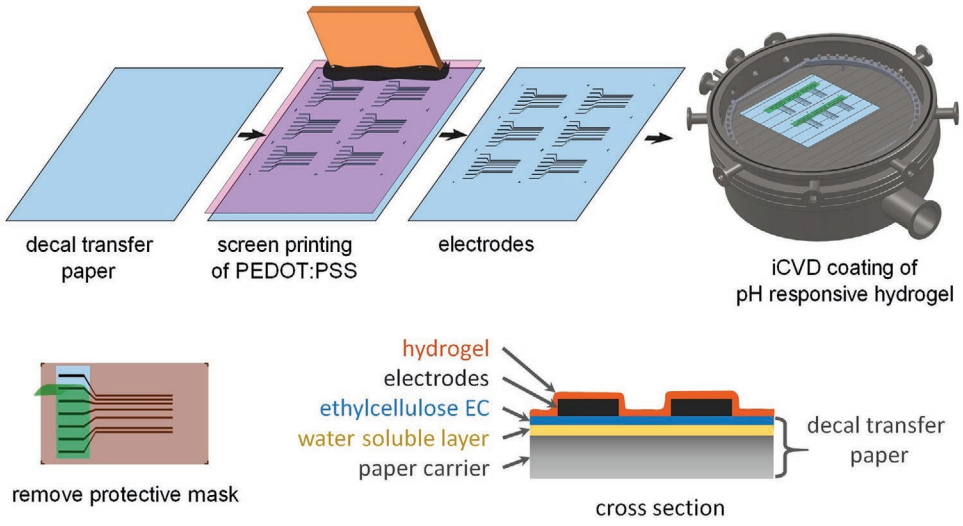

Figure 1. Fabrication steps of the pH sensor tattoo. The decal paper of a transferable temporary tattoo is used as a substrate. PEDOT:PSS electrodes are printed on the substrate via screen printing. A pH-responsive hydrogel (pMAA) is deposited via iCVD. Kapton tape is utilized to mask areas from unwanted deposition. After removal of the mask, the pH sensor tattoo can be transferred on skin, by applying a little pressure and wetting the back paper. A cross-section is pictured of the final pH sensor tattoo with all implemented layers within, the decal paper consisting of a paper carrier, a water soluble layer and the ethylcellulose EC layer, the polymer electrodes, and the pH-responsive hydrogel.

already used in other reports of tattoo sensors.[37] After the temporary tattoo paper was screen printed with PEDOT:PSS electrodes and further coated via iCVD with a co-polymer consisting of methacrylic acid (MAA) and di(ethylene glycol) divinyl ether (DEGDVE), the resulting pH sensor tattoo was thoroughly investigated concerning transferability, morphology, and chemistry.

2.1. Transferability

In **Figure 2**a, a cut-out part of the sensor applied on a silicon wafer and on a silicone replica of thumb epidermis can be seen. The transfer on the wafer was performed via floating technique, which led to a structure where the ethylcellulose layer is facing the wafer while the hydrogel and the electrodes (and the Ag coating provided for scanning electron microscope (SEM) imaging) are facing toward the microscope. Except the outlines, where the sensor was cut with a scissor which resulted in a frayed edge and some small areas with particles beneath the layer, the tattoo sensor is well adhered to the wafer. Clearly the electrodes can be seen as dark gray lines. As well the transition from the coated hydrogel to the part which was shielded during the deposition is visible as a distinct line. The shielded area looks completely uncoated in the SEM image. The possibility that the sensing part of the sensor can also face outward from a surface onto which the tattoo has been transferred lead to other possible methods of usage.

On the thumb replica, the sensor was transferred by pressing the sensor facing the hydrogel layer toward the replica, wetting the back paper, and removing the paper carrier sheet, resulting in a contact of the hydrogel with the silicone replica while the ethylcellulose layer is facing the microscope (see Figure 2b). Again, both the electrodes and the hydrogel can be seen. All areas within the sensor tattoo, namely, the hydrogel, the electrodes, and the uncoated tattoo follow the topological features of the thumb replica resulting in an intimate contact between the surface of the thumb and the sensor. Therefore, it can be concluded that coating a tattoo with PEDOT:PSS electrodes via screen printing and further with a co-polymer of MAA and DEGDVE (p(MAA-DEGDVE)) by iCVD compromise neither the transferability nor the ability to smoothly follow the underlying surface topography.

2.2. Morphology

Atomic force microscopy (AFM) was utilized to investigate the surface morphology of the different layers of the sensor tattoo. Again, the tattoo sensor was transferred via floating technique onto a Si wafer. In Figure 2c, the AFM topography image of all areas within the sensor is displayed. While the edge of the printed electrode is distinct and clearly visible, that of the hydrogel has some spikes at the border, due to irregularities at the protective mask. Indeed, during the iCVD deposition, one

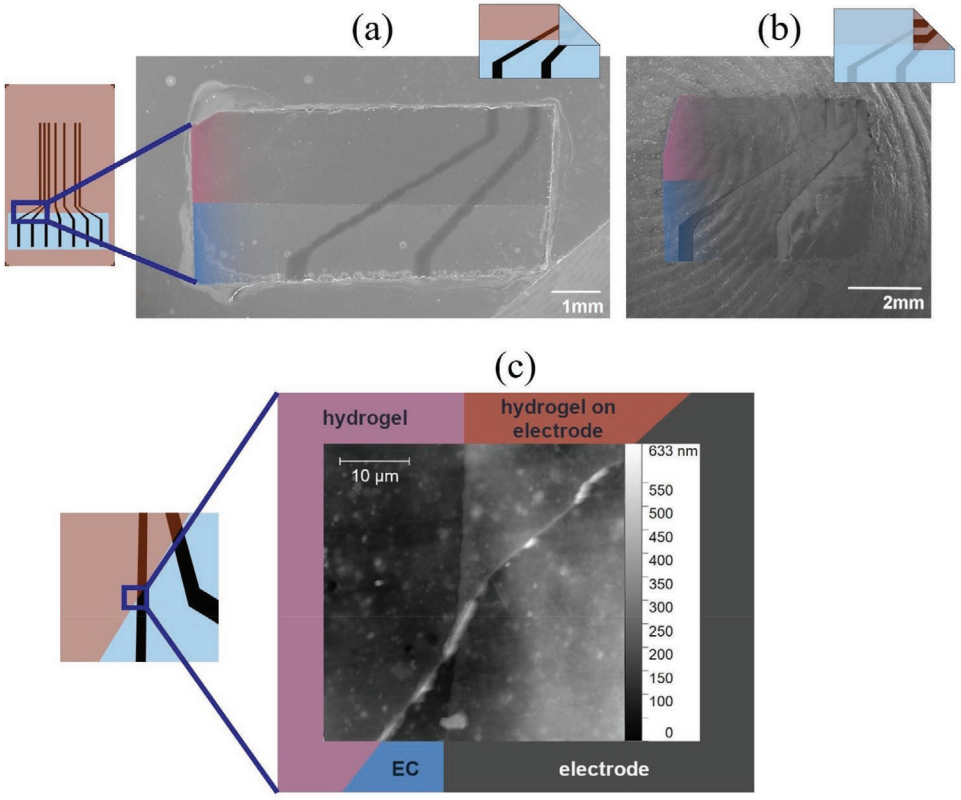

Figure 2. a) SEM image of a pH sensor tattoo transferred onto a Si wafer. The sensing part faces out of plane. b) Image of the pH sensor tattoo transferred on a silicone replica of thumb skin. The sensing part faces the thumb. c) AFM topography image of the four areas within the sensor tattoo. The surfaces of EC, hydrogel, and hydrogel on electrode have been color-coded for clarity: the EC surface is blue, the hydrogel surface is violet, and the hydrogel on electrode surface is red. Some violet and blue shadows have been added also to the SEM picture to indicate the hydrogel and the EC, respectively.

part of the tattoo and the electrodes were masked via a tape which was peeled off after the deposition. The removal of the tape seems to cause very localized delamination (<1 µm lateral) and small peeling off effects (<300 nm in height) of the hydrogel toward the layer underneath. The roughness, calculated by the root mean square error (R_{rms}), of the uncoated ethylcellulose layer was 30 ± 3 nm. The hydrogel layer coated on the ethylcellulose has an R_{rms} = 25 ± 2 nm. The R_{rms} values of the electrode and the hydrogel deposited on the electrodes are 27 ± 2 and 33 ± 3 nm, respectively. The iCVD coating technique typically results in a uniform polymer thin film with a constant film thickness which preserves the roughness of the underlying layer through the polymer growth, as confirmed by these results.

The thicknesses of the individual layers of the sensor tattoo with removed paper carrier were measured with profilometry. In **Figure 3**a, the line-scans of individual layers were stacked for visualization purpose. The EC layer of the tattoo has an average height of 530 ± 50 nm which is in the typical range of production for this decal paper, i.e., 400–600 nm.[37] The estimated error is the roughness' root mean square error, which is slightly above the determined value with AFM. The average thickness of an EC/hydrogel bilayer is 730 ± 54 nm which implies an increase of thickness of 200 nm compared to the bare EC, which fits perfectly the desired deposition thickness monitored via laser interferometry on the reference wafer and estimated with spectroscopic ellipsometry after the deposition (203 ± 1 nm) during the deposition.

PEDOT:PSS electrodes were patterned with screen printing and had a thickness of 1230 ± 44 nm. The average thickness of the coated electrodes (PEDOT:PSS/hydrogel) rises to 1440 ± 93 nm which is again an increase of 210 nm caused by the hydrogel coating. The thickness of the deposited hydrogel is the same on the reference wafer, on the tattoo, and on the electrode, meaning that the iCVD deposition kinetics does not favor none of the three surfaces. The maximum overall thickness of the sensor, i.e., in the areas composed of EC/PEDOT:PSS/hydrogel layers, is around 2 µm; this low thickness is very relevant for achieving the necessary conformability and transpirability for on-skin application.

The height profile of a cross-section of an electrode without hydrogel coating is plotted in Figure 3b. The width of the electrode was measured with 0.40 ± 0.03 mm which fits the designed value of 0.4 mm well, validating the accuracy of screen-printing process. Cross-sections of electrodes coated with hydrogels show no significant difference with an evaluated width of 0.41 ± 0.02 mm.

2.3. Chemical Composition

To verify the retention of chemical groups of the hydrogel during the iCVD deposition, Fourier-transform infrared (FTIR) spectra were analyzed (see Figure 3d). The spectrum of the hydrogel p(MAA-DEGDVE) deposited on a silicon wafer has its most intense absorption band at 1720 cm^{-1} which can be attributed to C=O stretching of the functional group of MAA. Further peaks caused by C—H stretching and bending, which are typical for polymer backbones, can be found in the ranges of 3000–2800 and 1500–1350 cm^{-1}, respectively. A typical vinyl absorption band would be at 1650 cm^{-1} corresponding to the C=C stretching. The hydrogel spectrum has negligible absorption at that frequency verifying a complete conversion of the monomer species to the polymer. The

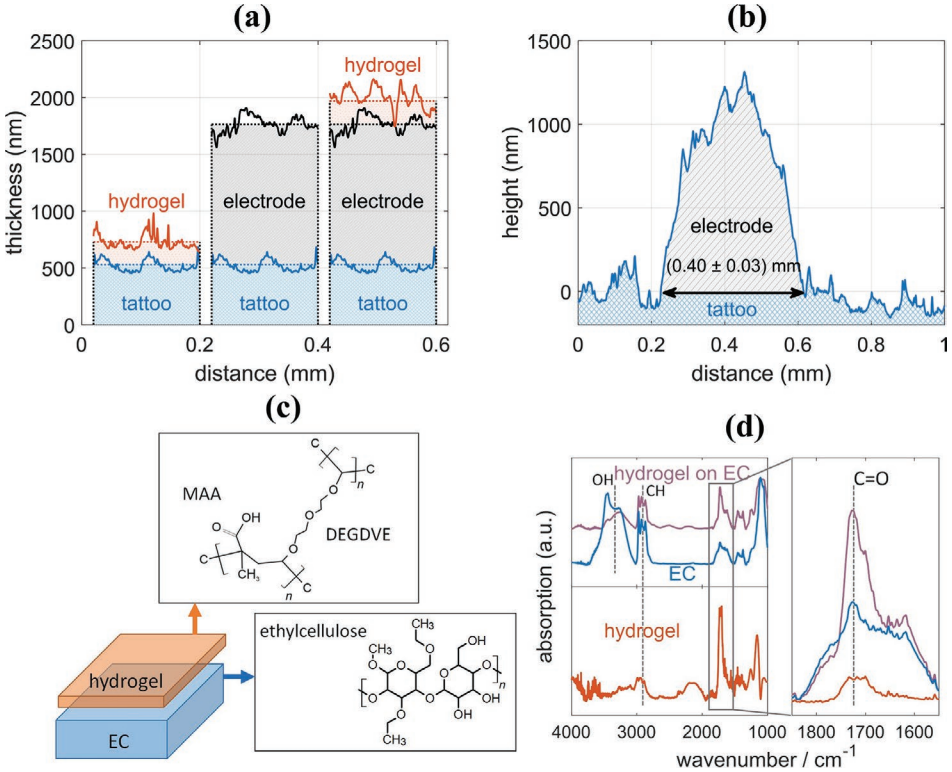

Figure 3. a) Thickness profiles of the different layers stacked above each other for visualization, as obtained by stylus profilometry. b) Height scan across a PEDOT:PSS electrode. c) Chemical structure of layers in the tattoo sensor: the native ethylcellulose layer releasable form a temporary tattoo paper, the screen-printed PEDOT:PSS, and the hydrogel. d) FTIR spectra of the hydrogel, the EC, and the EC/hydrogel.

IR spectrum of the ethylcellulose layer of the uncoated tattoo has a broad and intense O—H stretching absorption in the range of 3500–3150 cm^{-1}. After the deposition with p(MAA-DEGDVE), this peak got smaller which can be attributed to the affinity of the acid MAA group to deprotonate. Typically, the lost proton bounds to an -OH group which further became -OHH^+. Zooming into the fingerprint region, into the range of 1800–1600 cm^{-1}, shows that the uncoated tattoo absorbs exactly at 1720 cm^{-1}, way less than a coated tattoo. This can be explained by considering that the p(MAA-DEGDVE), which was deposited on the tattoo, also contributes to the adsorption at 1720 cm^{-1} with the C=O stretching of its ester groups. Concluding that the hydrogel is present on the tattoo and the chemistry of the hydrogel is also retained on the tattoo, which did not degrade during the deposition. After rinsing the coated tattoo with artificial sweat of pH 4 and pH 6, the absorption spectrum (not plotted) shows no change, indicating that the hydrogel did neither delaminate from the tattoo nor was chemically modified in the salty and acidic environment of artificial sweat.

3. pH Sensor Tattoo Responsiveness

3.1. pH-Responsive Swelling

Swelling response of the hydrogel in artificial sweat with changing pH values was measured in situ with spectroscopic ellipsometry. In **Figure 4**a, the upper plot schematizes the set pH value of the artificial sweat, which the sample was exposed to. After measuring the dry sample, the applied artificial sweat loops between pH 6 and pH 4, and during one loop also increases incrementally to evaluate the response in terms of responsiveness, repeatability, and sensitivity.

In dry state, the hydrogel thickness was evaluated with 203 ± 1 nm. With immersing the hydrogel in artificial sweat of pH 6, the thickness increases within 10 min to 277 ± 2 nm, which is a thickness increase of 36.5 ± 0.7% with respect to dry state. Changing the pH from 6 to 4 leads to a deswelling, resulting in a thickness increase of 24.3 ± 0.5% in respect to the dry state. Generally, acid groups within pH-responsive hydrogels have an association constant p$K\alpha$. With a pH value above p$K\alpha$, the acid groups deprotonate, resulting in a repulsion of the negative left acid groups; the hydrogel opens voids where water molecules can penetrate into and swells. Below p$K\alpha$, the acid groups protonate which results in a strong attraction among the acid groups and the hydrogel collapses (Figure 4c). Polymers of MAA have p$K\alpha$ values from pH 4.4 to pH 6.[63] The co-polymer hydrogel p(MAA:DEGDVE) de-swells when changing from pH 6 to pH 4 as a result of the protonation of the acid groups, as explained above. But at pH 4, the hydrogel is not in a complete shrunken state and has still a high swelling, implying that the hydrogel has also at pH 4 a good affinity to incorporate the artificial sweat. This can be explained by the interaction of the hydrogel with the salt as well as the attraction of the DEGDVE to water molecules.

When again looping the pH of the artificial sweat from pH 6 to pH 4, the hydrogel swells again to 37.0 ± 0.7% and shrinks back to 24.6 ± 0.5%, respectively. The swelling of the hydrogel is pH-responsive and reversible. Generally, the swelling of a pH-responsive hydrogel versus the pH is a sigmoid function, with the acid's dissociation constant p$K\alpha$ being defined as the inflection point of the curve (Figure 4c). Plotting the thickness

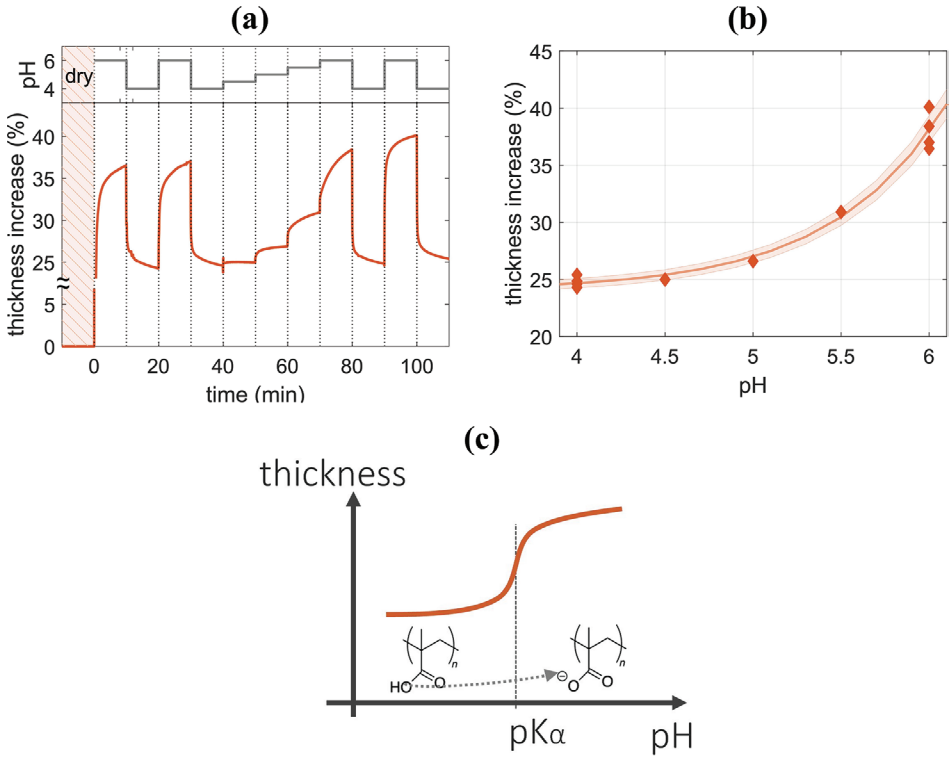

Figure 4. a) pH-responsive swelling of the hydrogel. b) Swelling (thickness increase, %) versus pH. c) Swelling behavior of a pH-responsive hydrogel in the pH domain around the inflection point, represented by p$K\alpha$ of MAA.

increase reached within 10 min versus the pH value (Figure 4b), the trend appears exponential implying that the p$K\alpha$ value of the synthesized hydrogel is not within the range from pH 4 to pH 6 but above. The swelling curves shift in time to slightly higher values (see Figure S1, Supporting Information). Such drifts may be explained by the cycled exposure to different pH values and the hydrogels improving reaction in terms of approaching the minimum in the free energy.

3.2. pH-Responsive Dielectric and Ion Conductivity Properties

To evaluate the dielectric and conductivity properties of the sensor tattoo, impedance spectra were taken. As representative of a series of measurements, the Bode plots of uncoated and hydrogel-coated tattoos immersed in artificial sweat at pH 6 and at pH 4 are plotted. In the Bode plots of the impedance (see **Figure 5**a), the absolute value of the impedance *Zmod* increased with increasing frequency in all the investigated samples.

In the frequency region from 10 to 1000 Hz, the *Zmod* of a coated tattoo immersed in pH 4 has a plateau at 7.1 ± 0.3 Ω, with the error being the deviation within the plateau. The plateau rises to 15.7 ± 0.7 Ω when the sample is exposed to pH 6, resulting in a pH-responsive change of *Zmod* of 215% within the pH range. Above 1000 Hz, *Zmod* increases and the pH responsiveness is lost. The *Zmod* of the uncoated tattoo increases from 10 to 700 Hz and reaches there a plateau at 42.8 ± 0.4 and 36.0 ± 0.6 Ω in pH milieu of pH 4 and pH 6, respectively. PEDOT:PSS itself is also pH-responsive with a dissociation constant p$K\alpha$ of 2.9. Although the p$K\alpha$ value is way below the used region, the evaluated pH response of *Zmod* was 20%. Above 10 kHz, the *Zmod* increases again for both curves and the pH responsiveness diminishes.

The Bode plot of the phase, which is the phase shift of the applied potential to the measured current sweep, of the four representative measurements are plotted in Figure 5b. At the frequency of 10 Hz, the phase of an uncoated tattoo immersed in solution of pH 6 is 38.0° ± 0.3°, which decreases reaching at 4000 Hz a local minimum of 5.8° ± 0.2°, and further increases again. When applying a solution of pH 4, the shape of the phase does not change but the curve is slightly shifted by about 2.5° to lower phases. A tattoo coated with a hydrogel in pH 6 has at 10 Hz a phase of 20° ± 1° which decreases till 300 Hz to 2.1° ± 0.3°, and further increases again. The same sample in pH 4 has a phase of 0° ± 0.3° at 10 Hz and rises continuously with frequency. The different shapes of the phase versus frequency of a tattoo coated with a hydrogel in either pH 4 or pH 6 are clearly visible and verify the pH-dependent dielectric properties of the coated sensor tattoo. At 120 Hz, the two curves intersect with each other. At this frequency, the phase shows no pH dependency.

A series of impedance spectroscopy measurements with varying the artificial sweat pH value were collected. The *Zmod* and the phase at frequencies of 10 and 1000 Hz for an uncoated tattoo were plotted in Figure 5c. The top row of the plot displays the set pH value. As the small difference of the phase curves of the uncoated tattoo already revealed, the pH dependency is barely visible and neglectably small. The *Zmod* is slightly pH dependent which converges after two times cycling between pH 6 and pH 4 to a *Zmod* of 40 ± 1 and 44.5 ± 0.5 Ω at pH 6 and pH 4, respectively. Nearly the same plot but with a coated sample instead is depicted in Figure 5d. A difference can be observed in the set pH values as also incremental steps between pH 4 and pH 6 were set during one loop. The phase exhibits a reversible pH response at both frequencies. At 10 Hz, the phase switches between 20° ± 1° and 0.3° ± 0.3° in pH 6 and pH 4, respectively. In contrast, the phase at 1000 Hz is as well pH responsive but flipped up to down with a phase of 3.6° ± 0.8° and 18° ± 1° in pH 6 and pH 4, respectively. The *Zmod* of the coated tattoo exhibits as well a pH responsive and reversible behavior at both frequencies. Varying between 7.2° ± 0.4° and 14° ± 2° for pH 4 and pH 6 at 10 Hz, respectively. And at 1000 Hz from 8.2° ± 0.5° to 17° ± 3° again for pH 4 and pH 6, respectively. Although the *Zmod* responsiveness toward pH (see Figure 5e) is with more than 200% of change rather high, the small response in the range of pH 4–5 as well as the large error of this parameter reduces its credibility as a trustworthy connection to the pH value. While on the contrary, the error of the phase is rather small (<1°) with an excellent pH responsiveness. The phase in respect to the pH value is plotted in Figure 5f. With increasing pH, the phase increases at 10 Hz and decreases at 1000 Hz.

The sensor's response stability was evaluated by comparing the phase when the pH level is changed from pH 4 to pH 6 and from pH 6 to pH 4 separately (see Figure S1, Supporting Information). When changing the pH from 4 to 6, the phase converges to slightly different values with a deviation of ± 1° (mean value is 5°). If the pH changes from 6 to 4, the phase converges reproducible with a slight deviation of ± 0.3° (mean value is 19.8°). When comparing the obtained deviation to the deviation of swelling of the hydrogel, again the change from pH 4 to pH 6 leads to a higher deviation of ± 1% (mean value of 38%), and a more reproducible converged thickness when the pH changes from pH 6 to pH 4 with a deviation of ± 0.3% (with a mean value of 24.7%) (see Figure 4b). While the change from a collapsed to an opened hydrogel structure converges to slightly different values of phase and thickness, the revise transformation results in a reproducible phase and thickness.

The response time (estimated with the time, the data point within the curve exceeds the 1/e factor between converging, and initial phase or swelling term, see Figure S1, Supporting Information) of the phase is 0.780 ± 0.002 and 1.2 ± 0.6 min, when the pH level is changed from 4 to 6 and from 6 to 4, respectively, which is in the limitation of time resolution, as one measurement takes about 0.78 min. The response time of the swelling is 0.36 ± 0.3 and 0.824 ± 0.003 min when the pH level changes from 4 to 6 and from 6 to 4, respectively. This suggests that the collapse of the hydrogel takes kinetically longer compared to the transition into an opened structure. This fast response may also explain the less reproducible phase and thickness when the pH changes from 4 to 6. Nevertheless, it should be mentioned here that although the sensor has a quick response to a relatively substantial pH change, the response time to little sweat production was not measured within this study.

Comparing the pH-responsive swelling of the hydrogel with the pH-responsive phase shift of the tattoo coated with the hydrogel permits the conclusion that the dielectric properties is correlated with the swelling.

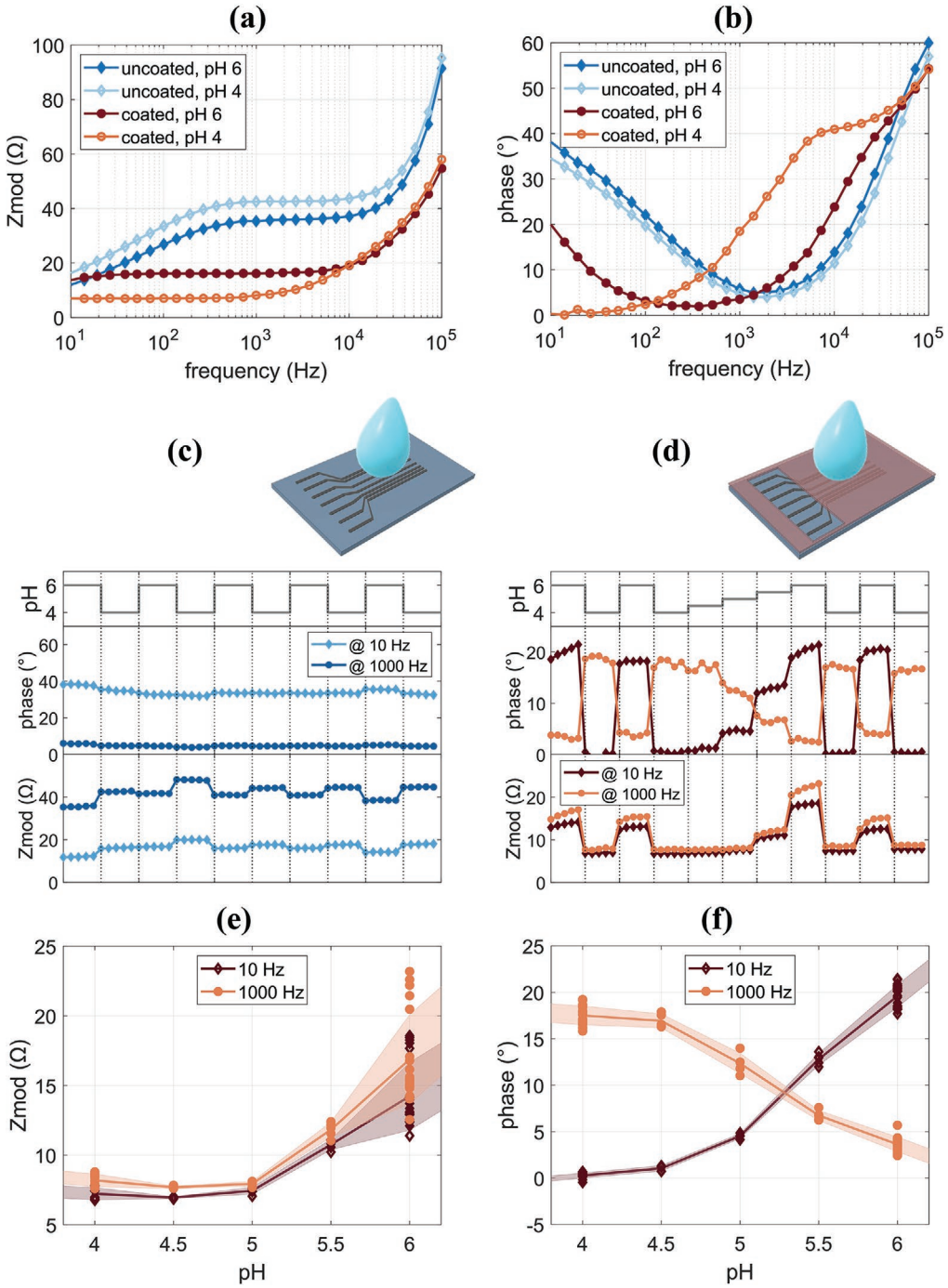

Figure 5. a) Bode plot of the impedance of the coated, and uncoated tattoo immersed in artificial sweat of pH 4 and pH 6. b) Bode plot of the phase with the same measurement. c) Schematic of the uncoated tattoo. *Zmod* and phase shift at 10 and 1000 Hz evaluated at different pH with an uncoated tattoo. d) Schematic of a tattoo coated with a hydrogel. *Zmod* and phase shift at 10 and 1000 Hz evaluated at different pH with a coated tattoo. e) *Zmod* versus pH at 10 and 1000 Hz for a coated tattoo. f) Phase shift versus pH at 10 and 1000 Hz for a coated tattoo.

4. pH Sensor Tattoo in Action

To close the gap between laboratory environment toward real time measurements of pH of human body, several challenges, such as determining the responsiveness to different analytes or amounts of sweat, a durable electrical connection from the sensor on the body to an outer device, or the development of an easy and cheap read-out hardware and software, need to be faced. Within this study, only the third of the mentioned objectives are addressed. A microcontroller

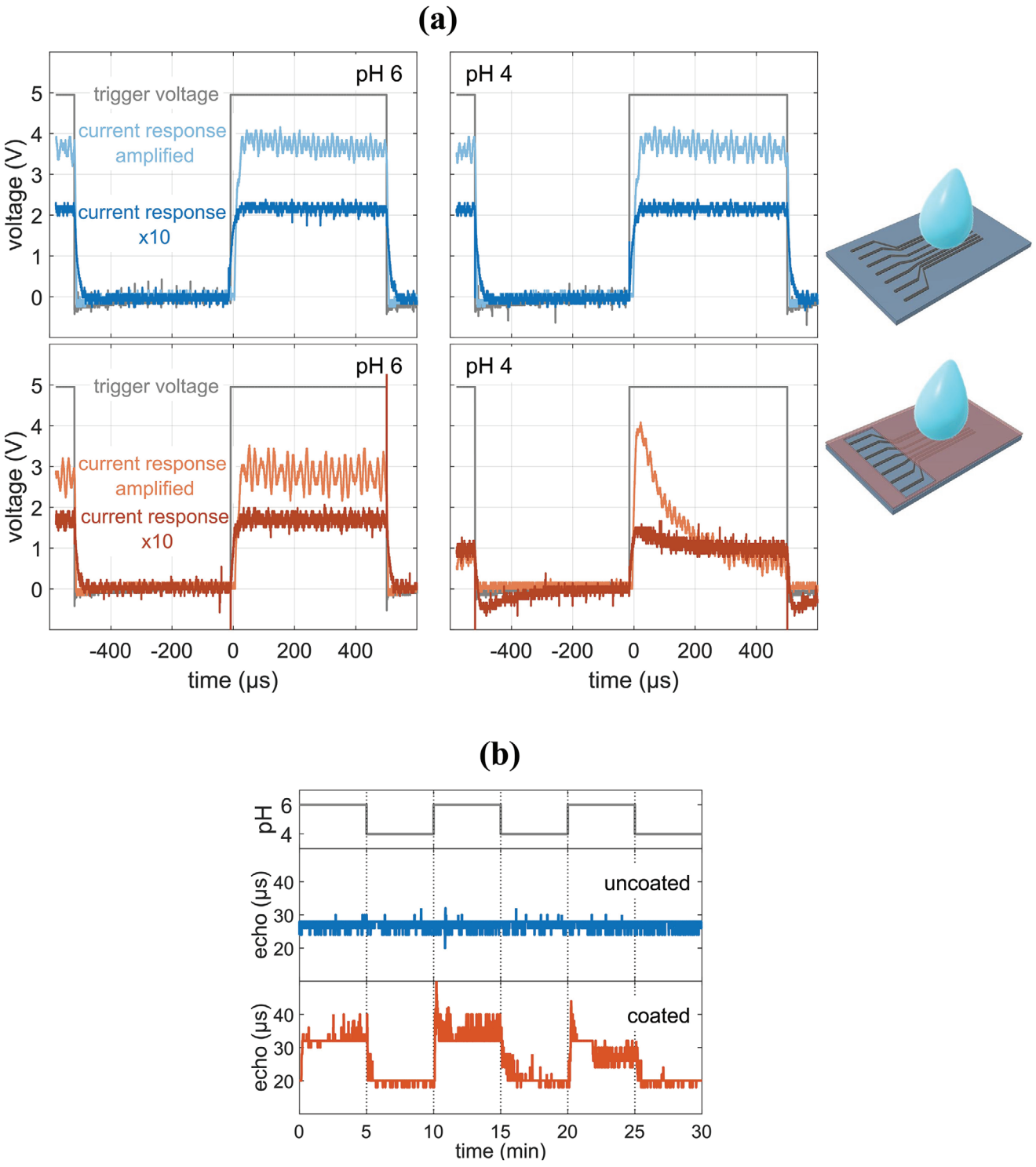

Figure 6. a) Oscilloscope measurement of the trigger voltage, the current response, and the amplified current response of an uncoated and coated tattoo in artificial sweat of pH 4 and pH 6. b) Echo time, which is the time between the positive edge of the trigger and the current response in artificial sweat of pH 4 and pH 6.

(Arduino) was used as signal generator and read-out terminal for the current response. In **Figure 6**a, an oscilloscope visualized the signals of the uncoated tattoo in artificial sweat of pH 6 and pH 4, and a tattoo coated with a hydrogel at pH 6 and pH 4. Within one of these plots, the applied voltage sweep, the current response (converted to a voltage signal), and further amplified current signal can be seen. While the uncoated sample seems to have no response toward the pH value,

the coated tattoos reply is linkable to the set pH. At pH 6, the current response rises after the positive edge and converges then to a constant value. At the falling edge, the signal decays exponentially back to 0 V. In contrary, at pH 4 the current response increases till a local maximum and decreases again converging to a constant value. At the falling edge, the current response decays below zero, passes a negative peak, and converges to zero again. After this signal got further amplified, which was needed to get a measurable signal for the Arduino, the peak got pronounced and the signals below 0 V got lost (because it was a rail-to-rail amplifier which can only operate above 0 V), which can only be ascribed to the nonlinear behavior of the chosen amplifier. The demand of amplifiers within the detection strategy of the sensor can be seen as a drawback, as such components often lead to a broad noise, which can be seen in Figure 6a, when looking at the amplified data.

The echo measured by the Arduino, which is the time between the positive voltage edge to the current response, versus the pH value is depicted in Figure 6b. In the first row, the set pH value switching between 6 and 4 is plotted. While the echo of the uncoated tattoo has no pH dependency, the echo of the coated tattoo responds well to the artificial sweat pH.

In retrospective, the hardware and software could have been easily improved (Arduino due—faster, different amplifier + upconverter—to also be able to measure the negative response or simply tracking data points of the analog signal and evaluate the shape), which would enhance the gained response quality, but already this simple attempt led to a measurable response which emphasizes the idea of a sensor tattoo that can easily be read out by nonsophisticated electronics.

5. Conclusions

A pH skin sensor tattoo was successfully fabricated by screen printing of PEDOT:PSS electrodes, and further depositing a pH-responsive hydrogel p(MAA-DEGDVE) via iCVD directly on a temporary tattoo substrate. During the fabrication, the applicability of the tattoo did not get compromised and the ability to conformally adhere to the complex topology of rough surfaces was retained. The measured electrode width 0.40 ± 0.02 mm fit excellent the designed value of 0.4 mm and the height of the electrode of 1230 ± 44 mm implies full retention of the ultra-thin features of the tattoo. The possibility to apply the sensor tattoo not only facing into the substrate but also in direction out of the substrate can lead to various application possibilities. The synthesis of the hydrogel layer by iCVD on the tattoo was proved. The obtained hydrogel has equal height (≈200 nm) on the reference wafer, the tattoo surface, and the electrode surface. Together the results bear out excellent controllability of the morphology during manufacturing process.

The pH-responsive swelling of the hydrogel layer was evaluated with a thickness increase of 38 ± 1% and 24.7 ± 0.3% in artificial sweat of pH 6 and pH 4, respectively, in respect to the dried state. The Bode plot of the impedance of the sensor tattoo coated with the hydrogel immersed in artificial sweat exhibits a pH-responsive shift of the plateau at the frequency range from 10 to 1500 Hz from 7.1 ± 0.3 to 15.7 ± 0.7 Ω at pH 4–6, respectively, which is about 215% increase. The uncoated tattoo in this plot is generally shifted to higher values and has also a pH-responsive shift from 42.8 ± 0.4 to 36.0 ± 0.6 Ω at pH 4–6, respectively. The Bode plot of the phase evidences distinct features of the sensor tattoo coated with the hydrogel at pH 4 and pH 6, while the uncoated sensor tattoo indicates no response toward the pH. The absolute value of the impedance and the phase shift at the frequency of 10 and 1000 Hz of the sensor tattoo subsequentially immersed in artificial sweat of different pH values were extracted. The selected value demonstrates for the sensor tattoo coated with hydrogel excellent reversible pH responsiveness while only little or no responsiveness of an uncoated sensor tattoo can be seen. The phase shift was identified as the best property to link to the pH.

In a self-made microcontroller setup, an Arduino was used as trigger and read-out terminal to demonstrate the sensors capability to be operated without sophisticated lab equipment.

6. Experimental Section

Device Fabrication and Mixture of Artificial Sweat: *Screen Printing of Electrodes*: The temporary transfer tattoo paper used in this study was commercially available (The Magic Touch Ltd., UK) and was composed of a decal transfer paper and a glue sheet. The decal transfer paper consists of a paper carrier sheet, a starch-dextrin water soluble layer, and an ethylcellulose layer. The glue sheet is made of a silicone paper carrier, an acrylic glue layer, and a plastic liner.

In this project, the decal transfer paper was used as substrate for screen printing PEDOT:PSS electrodes. To produce the pattern for the screen printing, an UV-curing emulsion (Ultra Coat 535, CPS—Chemical Products and Services, I&W Handels GmbH, Austria) was applied on the mesh (Saatilene, I&W Handels GmbH, Austria, mesh counts of 77T). The electrode design was printed on a print paper which acted as a mask during the UV illumination (time: 200 s, UVP Transilluminator PLUS, Analytik Jena AG, Germany). Afterward the screen was washed with water. The PEDOT:PSS ink (Clevios S V4 Stab, Heraeus, Germany) was re-dispersed before applying it on the decal transfer paper with a screen lift-off of 0 mm with one single move. An optical microscope image can be found in Figure S2 in the Supporting Information.

Hydrogel Coating via iCVD: The pH-responsive hydrogel coating was synthesized via iCVD in a custom built iCVD chamber, described elsewhere.[64] The monomer species were methacrylic acid (MAA, 99%, Merck, Darmstadt, Germany), di(ethylene glycol) divinyl ether (DEGDVE, 99%, Merck, Darmstadt, Germany), and the ethylene-glycol-dimethacrylate (EGDMA, 98%, Sigma Aldrich, Germany), and the initiator was *tert*-butyl peroxide (TBPO, 98%, Sigma Aldrich, Germany). The substrates, namely, a silicon wafer and the tattoo with the screen-printed PEDOT:PSS electrodes were kept at a temperature of 30 °C by a chiller/heater system (Thermo Scientific Accel 500 LC). All edges of the tattoo paper were taped by Kapton adhesive tape (Tesa 51808 Kapton) on the chamber bottom to prevent coating of the backside. Kapton adhesive tape was used also to mask the part of the tattoo electrodes that needed to be contacted afterward, for preventing their coating during the iCVD process. A photo of a loaded reactor is illustrated in Figure S3 in the Supporting Information. The temperature of the MAA, DEGDVE, and EGDMA monomer jars were set to 70, 70, and 85 °C, respectively, mixed in a heated line, and were further fed into the reactor chamber. The MAA, DEGDVE, EGDMA, and TBPO (unheated, separated line) flowrates were 4.4, 0.4, 0.2, and 1 sccm, respectively, set

by needle valves. The working pressure was set to 400 mTorr. Thermal decomposition of the initiator TBPO was induced via a hot filament 270 ± 10 °C of nickel-chromium wires (Goodfellow, UK). The deposition was started with only the EGDMA, and the TBPO line opened. After 2 min, the MAA and DEGDVE lines were additionally opened. Again after 2 min, the EGDMA line was closed. With this procedure, a strong adhesive bond from the polymer layer to the substrate could be expected which should prevent delamination. pEGDMA is an inert and rigid material, which does not swell or respond to artificial sweat. The transition layer p(MAA:DEGDVE:EGDMA) had a reduced swelling compared to p(MAA:DEGDVE). During the impedance measurements, the layers could be represented in an equivalent circuit as serial applied resistors parallel to capacitors. To this hypothesis, the properties of the representing pEGDMA layer equivalent element did not change with pH and the representing elements of p(EGDMA:MAA:DEGDVE) had a reduced response to pH. But due to the thickness of the interstitial layers thinner than 2 ± 1 nm, the reduction of response was only marginal.

The polymer thickness on the silicon wafer was in situ monitored by laser interferometry ((He–Ne Laser with λ = 633 nm, Thorlabs, USA). After a layer thickness of 200 nm, the deposition was terminated at 68 min deposition time.

Platform for Mounting the Ultra-Thin Tattoo via Printed Circuit Board: To connect to the electrodes and stabilize the tattoo when the paper carrier was removed, a printed circuit board (PCB) was designed and produced (Ni-Au coating, Eurocircuit, Germany). The PCB had on one side a shape that could be plugged into a 7 pole SATA cable (typically used to connect to hard drives) to easily connect the wires of the cable further to any kind of measuring device. In the middle, the PCB had a routed hole because the tattoo sensor surface was facing in direction of the PCB when it was connected. The hole acted like a compartment that made the sensor accessible, and could hold solutions within. Between the tattoo sensor and the PCB, the glue sheet of the tattoo was placed to improve the adhesion (the assembling routine is depicted in Figure S5, Supporting Information). The glue sheet was cut out via a laser cutter (ULS2.30, Universal Laser System equipped with a 30 W CO_2 laser source at 10.6 µm wavelength) removing the areas where the tattoo was not covered, namely, the sensor part in the middle and the part where the electrodes of the tattoo and of the PCB were connected.

Artificial Sweat: Artificial sweat was prepared based on the ISO 3160-0 recipe which was typically used for testing degradation processes of wearable body sensors. Milli-Q water was mixed with NaCl (Merck, Germany), NH_4Cl (Merck, Germany), acetic acid (Fluka >99.8%, 45731), and lactic acid (Sigma Aldrich, W 261106, 85%, Germany). The concentrations were: NaCl 20 g L^{-1}, NH_4Cl 17.5 g L^{-1}, acetic acid 5 g L^{-1}, and lactic acid 15 g L^{-1}. A solution of NaOH (150 g L^{-1}, Merck, Germany) in Milli-Q water was used to set the pH value. In contrast to the recipe, the pH value was not set to 4.7 but solutions at pH 4, 4.5, 5, 5.5, and 6 were prepared. These pH values were fit well the desired range of typical sweat, did not corrode any lab equipment, and provided a stable buffer solution.

Device Characterization Methods: *Applicability—SEM*: SEM imaging was used to observe the applicability of the sensor tattoo. For this purpose, one sample was produced via floating technique. A small part of the sensor tattoo was cut out with scissors and floated on the surface of demineralized water facing the carrier paper into the water. The starch-dextrin layer was dissolved and the paper carrier sheet sank while the ethylcellulose layer with the electrodes and the hydrogel layer remained floating on the water surface. With a silicon wafer, the sample was lifted from underneath out of the water. Photos of the floating transfer routine can be found in Figure S4 in the Supporting Information. A silver layer of 20 nm was physically vapor deposited with a thermal evaporator operating at a pressure of 1×10^{-3} mbar and at a deposition rate of 0.65 ± 0.1 A s^{-1}. The fingertip silicone replica was produced by first creating a negative of a fingertip made of clay (Fimo, Staedler Mars GmbH, Germany) which was further hardened by 110 °C for 30 min: then this negative was coated with polydimethylsiloxane (PDMS) (Dow Corning, United States, Silicone Elastomer Kit 1:10 mixing ratio curing agent to prepolymer), which was further cured at 85 °C for 2 h. After peeling the PDMS fingertip replica out of the negative, a cut-out piece of the sensor tattoo was placed on it facing the hydrogel toward the replica surface, wetted with demineralized water, and the paper carrier sheet was removed. SEM (Jeol JSM-6490LV, Labco GmbH, Pressbaum, Austria) images were recorded at 10 and 20 keV acceleration voltage.

Morphology—AFM and Profilometry: AFM was utilized to get insight about the morphology properties of all surfaces present in the tattoo sensor. A Nanosurf easyScan 2 AFM equipped with a PPP-NCLR-10 cantilever and operating in tapping mode was used. The scanned area was set to 50 × 50 μm^2, the time per line to 1.2 s, the points per line to 512, the setpoint to 60%, the P-gain to 3500, the D-gain to 1000, and the vibration amplitude to 180 mV. AFM imaging was carried out on the surface of a tattoo transferred onto a silicon wafer via the floating technique described previously.

The thickness of the individual layers of the sensor tattoo was measured with an AlphaStep D-500 Profilometer from KLA-Tencor. The sensor tattoo was transferred onto a silicon wafer. Line scans were taken starting on the silicon wafer and crossing the step onto different surfaces of the sensor tattoo, namely, the EC layer, the EC coated with the hydrogel p(MAA-DEGDVE), the screen-printed electrodes (PEDOT:PSS) on EC, and the EC/PEDOT:PSS/hydrogel trilayer. Profilometry scanning parameters were set to: speed 0.05 mm s^{-1}, scan length 0.5 mm, stylus force 0.2 mg. Additional cross-section scans of the electrodes were performed with scanning properties as followed: scan speed 0.1 mm s^{-1}, scan length 1 mm, stylus force 0.2 mg. The width was measured between the spots where the declining electrode exceeded the height of 0 nm. Three electrodes were measured to get the statistical error.

Chemical Composition—Infrared Spectroscopy: The chemical composition within the hydrogel was measured with FTIR spectroscopy with a Michelson interferometer (Bruker IFS 66v/S) in transmission mode. The measurement chamber was kept at a vacuum of about 5 mbar to prevent absorption from air. Measurements of spectra were taken from a bare silicon wafer, a wafer coated with the hydrogel p(MAA-DEGDVE), an EC layer transferred from a temporary tattoo paper, a transferred EC/hydrogel tattoo, and the same sample but after immersing it for 15 min in pH 4 and for 15 min in pH 6 to verify the chemical retention after the acid environment. The spectrum of the wafer coated with the hydrogel was divided by the silicon wafer to obtain the hydrogel layers absorption only. The scan properties were chosen as followed, resolution 4 cm^{-1}, scan-time 1000 scans, range 4000–500 cm^{-1}, aperture 8 mm.

pH-Responsive Swelling—Ellipsometry: The film thickness of the hydrogel upon swelling in artificial sweat at different pH values was measured with spectroscopic ellipsometry (J. A. Woollam ESM-3000, Lincoln, NE, USA). A tight sealed liquid cell (J. A. Woollam, Lincoln, NE, USA) was used to expose the sample to the different solutions while in situ spectra were taken each 4 s at an angle of 75° in the spectral region from 370 to 1000 nm. Each 10 min the artificial sweat within the cell (cell volume about 4 mL) was exchanged by injecting 10 mL of artificial sweat at different pH values into the inlet of the cell. At the outlet, the drained solution was tested with a pH indicator paper to verify the complete change of the pH to the desired new value.

pH-Responsive Dielectric Properties—Electrochemical Impedance Spectroscopy (EIS): To take EIS measurements, the tattoo sensor was mounted on the designed PCB and the paper carrier sheet was removed. The PCB was connected to a SATA 7 plug-in where on the other side the cables were unshielded, and further connected to the working, working sense, reference, and counter electrode of a Gamry Instrument (Reference 600). The setup is depicted in Figure S6 in the Supporting Information. Artificial sweat solutions of different pH were subsequently inserted into the PCBs compartment area. Galvanostatic EIS measurements were performed in the frequency range of 10 Hz – 100 kHz, with a resolution of 7 points per decade, with an AC current of 10^{-5} A, and no offset DC current. The reproducibility of the electrochemical investigation was tested by repeating the characterization on a second tattoo replica. The resulting shapes and values of the Bode plots as well as the pH-responsive behavior could be successfully reproduced,

see Figure S7 in the Supporting Information. The galvanostatic measurement did not cause a drift of the applied voltage as can be seen in Figure S8 in the Supporting Information.

Arduino as Trigger and Read-Out Terminal: To prove that the sensor could be operated also with cheap and nonsophisticated equipment, in a first attempt a microcontroller (Arduino Uno) was used as a terminal platform. An output pin of the Arduino generated a pulsed signal with 50% duty cycle with a frequency of 1 kHz between 0 and 5 V. As PEDOT:PSS started to chemically oxidize or reduce above 100 mV, the voltage signal was down transformed via a voltage bridge to 7 mV which was pinned to the first electrode of the sensor tattoo. The second electrode was connected with a micro-current device, which was a self-made electronic device that was capable of transferring nA current signals to a voltage signal between −3 and 3 V, which was further connected to common ground. The output voltage signal of the micro-current device needed to be further increased, which was done by a rail-to-rail amplifier operated in noninverting amplification mode. After that, the signal was pinned back to a digital input of the Arduino. A schematic of the project and the micro-current device circuit diagram is illustrated in Figures S9 and S10 in the Supporting Information. In this configuration, the applied voltage sweep could be compared with the resulting current response. Because the experimental results of the electrochemical impedance spectra identified the phase as the most reliable parameter to be able to link to a pH, the echo, which was the time between the applied positive voltage signal edge till the current response reached a threshold (the Arduino code can be found in the Supporting Information). To track the signal sweep of the applied voltage, the voltage signal after the micro-current device, which should be directly linked to the current response, and the further amplified voltage signal directly before the Arduino input, an oscilloscope was utilized.

Statistical Analysis: *AFM*: Data were afterward leveled, and the statistical data were evaluated via the software Gwyddion. The roughness R_{rms} was calculated as the RMS error in respect to the average height function of a chosen area.

Profilometry: Data were afterward leveled via the native software of the instrument. The statistical evaluation of the height and the roughness were calculated taking the line scan after the border of the step and calculating the average and the RMS deviation of the height.

FTIR: All spectra were afterward baseline corrected.

Ellipsometry: The spectrum of the hydrogel in dry state (measured in air) was fitted with a three-layer model consisting of a silicon substrate, a native silicon dioxide (2 nm), and a Cauchy layer, representing the hydrogel. The obtained parameters were the thickness and the error of the thickness. While measuring in artificial sweat, the Cauchy layer was replaced by an effective material approximation model, which averaged the defined optical properties of two different materials weighted by the materials ratio within the layer. One material optical properties were the parameters obtained for the hydrogel in dried state and the other material was water. The thickness and the error of this layer and the ratio of the two materials were then the only fitting parameters. This is a typical procedure for transparent swollen hydrogels. The plotted swelling curves are a relation of the thickness in swollen state to the thickness in dried state ($100 \cdot t_{swollen}/t_{dry} - 100$).

Swelling versus pH: Thickness increase after 10 min of each cycle was extracted and plotted versus the pH value. The data were fitted via Matlab with an exponential curve of the form $a+b \cdot \exp(c \cdot (x-4))$. The error of the fit versus the pH was calculated with the covariance-matrix C and was plotted as a shaded area toward the fit.

Impedance Spectroscopy: The extracted *Zmod* and phase values together with the deviations was determined by averaging five measurements.

Impedance versus pH: *Zmod* and the phase, both at 10 and 1000 Hz, were plotted versus the pH. The mean value and the standard deviation for each pH value were calculated and plotted as a shaded area together with the scatterplot and the mean value.

Response Stability and Response Time: The swelling and phase curves, when the sample was exposed to a different pH value, were fitted with Matlab with an exponential function with the form $a+b \cdot \exp(c(x+d))$, with a, b, c, and d as fitting parameter. The response stability mean value and standard deviation were calculated by averaging the conversion value of these curves, when the sample was exposed to the same change of pH values. The response time was estimated by extracting the time, the data point within the curve exceeded the 1/e factor between converging and initial phase or swelling term.

Arduino Echo Time: The echo time was smoothed by Matlab via the smoothdata function with the movmedian method, which extracted the median within a certain data window, which was set to 6.

Supporting Information

Supporting Information is available from the Wiley Online Library or from the author.

Acknowledgements

The project has received funding from the Women in Science fellowship by L'Oréal and the UNESCO.

Conflict of Interest

The authors declare no conflict of interest.

Data Availability Statement

The data that supports the findings of this study are available from the corresponding author upon reasonable request.

Keywords

Arduino, biomonitoring, iCVD, smart hydrogel, wearable device

Received: June 14, 2021
Revised: August 6, 2021
Published online: November 10, 2021

[1] Y. Ling, T. An, L. W. Yap, B. Zhu, S. Gong, W. Cheng, *Adv. Mater.* **2020**, *32*, 1904664.
[2] Kenry, J. C. Yeo, C. T. Lim, *Microsyst. Nanoeng.* **2016**, *2*, 16043.
[3] T. Q. Trung, N. E. Lee, *Adv. Mater.* **2016**, *28*, 4338.
[4] T. Someya, M. Amagai, *Nat. Biotechnol.* **2019**, *37*, 382.
[5] Y. Gao, L. Yu, J. C. Yeo, C. T. Lim, *Adv. Mater.* **2020**, *32*, 1902133.
[6] S. Han, J. Kim, S. M. Won, Y. Ma, D. Kang, Z. Xie, K. T. Lee, H. U. Chung, A. Banks, S. Min, S. Y. Heo, C. R. Davies, J. W. Lee, C. H. Lee, B. H. Kim, K. Li, Y. Zhou, C. Wei, X. Feng, Y. Huang, J. A. Rogers, *Sci. Transl. Med.* **2018**, *10*, eaan4950.
[7] H. R. Lim, H. S. Kim, R. Qazi, Y. T. Kwon, J. W. Jeong, W. H. Yeo, *Adv. Mater.* **2020**, *32*, 1901924.
[8] K. Mitsubayashi, T. Arakawa, *Electroanalysis* **2016**, *28*, 1170.
[9] D. Pankratov, E. González-Arribas, Z. Blum, S. Shleev, *Electroanalysis* **2016**, *28*, 1250.
[10] A. Tricoli, N. Nasiri, S. De, *Adv. Funct. Mater.* **2017**, *27*, 1605271.
[11] J. Heikenfeld, *Electroanalysis* **2016**, *28*, 1242.
[12] M. Bariya, H. Y. Y. Nyein, A. Javey, *Nat. Electron.* **2018**, *1*, 160.
[13] J. Choi, R. Ghaffari, L. B. Baker, J. A. Rogers, *Sci. Adv.* **2018**, *4*, eaar3921.

[14] Y. Song, J. Min, Y. Yu, H. Wang, Y. Yang, H. Zhang, W. Gao, *Sci. Adv.* **2020**, *6*, eaay9842.
[15] E. Proksch, *J. Dermatol.* **2018**, *45*, 1044.
[16] H. Lambers, S. Piessens, A. Bloem, H. Pronk, P. Finkel, *Int. J. Cosmet. Sci.* **2006**, *28*, 359.
[17] E. Kim, S. Kim, G. W. Nam, H. Lee, S. Moon, I. Chang, *Int. J. Cosmet. Sci.* **2009**, *31*, 263.
[18] S. Anastasova, B. Crewther, P. Bembnowicz, V. Curto, H. M. Ip, B. Rosa, G. Z. Yang, *Biosens. Bioelectron.* **2017**, *93*, 139.
[19] H. Y. Y. Nyein, L. C. Tai, Q. P. Ngo, M. Chao, G. B. Zhang, W. Gao, M. Bariya, J. Bullock, H. Kim, H. M. Fahad, A. Javey, *ACS Sens.* **2018**, *3*, 944.
[20] W. Dang, L. Manjakkal, W. T. Navaraj, L. Lorenzelli, V. Vinciguerra, R. Dahiya, *Biosens. Bioelectron.* **2018**, *107*, 192.
[21] S. Nakata, M. Shiomi, Y. Fujita, T. Arie, S. Akita, K. Takei, *Nat. Electron.* **2018**, *1*, 596.
[22] H. Y. Y. Nyein, W. Gao, Z. Shahpar, S. Emaminejad, S. Challa, K. Chen, H. M. Fahad, L. C. Tai, H. Ota, R. W. Davis, A. Javey, *ACS Nano* **2016**, *10*, 7216.
[23] M. Tessarolo, I. Gualandi, B. Fraboni, *Adv. Mater. Technol.* **2018**, *3*, 1700310.
[24] W. He, C. Wang, H. Wang, M. Jian, W. Lu, X. Liang, X. Zhang, F. Yang, Y. Zhang, *Sci. Adv.* **2019**, *5*, eaax0649.
[25] L. M. Ferrari, S. Sudha, S. Tarantino, R. Esposti, F. Bolzoni, P. Cavallari, C. Cipriani, V. Mattoli, F. Greco, *Adv. Sci.* **2018**, *5*, 1700771.
[26] A. Zucca, C. Cipriani, Sudha, S. Tarantino, D. Ricci, V. Mattoli, F. Greco, *Adv. Healthcare Mater.* **2015**, *4*, 983.
[27] J. Choi, D. Kang, S. Han, S. B. Kim, J. A. Rogers, *Adv. Healthcare Mater.* **2017**, *6*, 1601355.
[28] X. He, T. Xu, Z. Gu, W. Gao, L. P. Xu, T. Pan, X. Zhang, *Anal. Chem.* **2019**, *91*, 4296.
[29] S. Wang, Y. Wu, Y. Gu, T. Li, H. Luo, L. H. Li, Y. Bai, L. Li, L. Liu, Y. Cao, H. Ding, T. Zhang, *Anal. Chem.* **2017**, *89*, 10224.
[30] L. Manjakkal, S. Dervin, R. Dahiya, *RSC Adv.* **2020**, *10*, 8594.
[31] J. R. Windmiller, A. J. Bandodkar, G. Valdés-Ramirez, S. Parkhomovsky, A. G. Martinez, J. Wang, *Chem. Commun.* **2012**, *48*, 6794.
[32] A. J. Bandodkar, W. Jia, C. Yardimci, X. Wang, J. Ramirez, J. Wang, *Anal. Chem.* **2015**, *87*, 394.
[33] J. Kim, W. R. De Araujo, I. A. Samek, A. J. Bandodkar, W. Jia, B. Brunetti, T. R. L. C. Paixão, J. Wang, *Electrochem. Commun.* **2015**, *51*, 41.
[34] A. J. Bandodkar, V. W. S. Hung, W. Jia, G. Valdés-Ramírez, J. R. Windmiller, A. G. Martinez, J. Ramírez, G. Chan, K. Kerman, J. Wang, *Analyst* **2013**, *138*, 123.
[35] J. Kim, I. Jeerapan, S. Imani, T. N. Cho, A. Bandodkar, S. Cinti, P. P. Mercier, J. Wang, *ACS Sens.* **2016**, *1*, 1011.
[36] T. Guinovart, A. J. Bandodkar, J. R. Windmiller, F. J. Andrade, J. Wang, *Analyst* **2013**, *138*, 7031.
[37] L. M. Ferrari, K. Keller, B. Burtscher, F. Greco, *Multifunct. Mater.* **2020**, *3*, 032003.
[38] A. J. Bandodkar, W. Jia, J. Wang, *Electroanalysis* **2015**, *27*, 562.
[39] G. E. Bonacchini, C. Bossio, F. Greco, V. Mattoli, Y. H. Kim, G. Lanzani, M. Caironi, *Adv. Mater.* **2018**, *30*, 1706091.
[40] Z. Sonner, E. Wilder, J. Heikenfeld, G. Kasting, F. Beyette, D. Swaile, F. Sherman, J. Joyce, J. Hagen, N. Kelley-Loughnane, R. Naik, *Biomicrofluidics* **2015**, *9*, 031301.
[41] G. S. Rekhi, S. S. Jambhekar, *Drug Dev. Ind. Pharm.* **1995**, *21*, 61.
[42] M. E. Alf, A. Asatekin, M. C. Barr, S. H. Baxamusa, H. Chelawat, G. Ozaydin-Ince, C. D. Petruczok, R. Sreenivasan, W. E. Tenhaeff, N. J. Trujillo, S. Vaddiraju, J. Xu, K. K. Gleason, *Adv. Mater.* **2010**, *22*, 1993.
[43] A. M. Coclite, R. M. Howden, D. C. Borrelli, C. D. Petruczok, R. Yang, J. L. Yagüe, A. Ugur, N. Chen, S. Lee, W. J. Jo, A. Liu, X. Wang, K. K. Gleason, *Adv. Mater.* **2013**, *25*, 5392.
[44] W. E. Tenhaeff, K. K. Gleason, *Adv. Funct. Mater.* **2008**, *18*, 979.
[45] K. K. S. Lau, K. K. Gleason, *Macromolecules* **2006**, *39*, 3688.
[46] K. K. S. Lau, K. K. Gleason, *Macromolecules* **2006**, *39*, 3695.
[47] H. J. Park, S. J. Yu, K. Yang, Y. Jin, A. N. Cho, J. Kim, B. Lee, H. S. Yang, S. G. Im, S. W. Cho, *Biomaterials* **2014**, *35*, 9811.
[48] H. S. Lee, H. Kim, J. H. Lee, J. B. Kwak, *Coatings* **2019**, *9*, 430.
[49] K. Unger, A. M. Coclite, *Pharmaceutics* **2020**, *12*, 904.
[50] G. Decandia, F. Palumbo, A. Treglia, V. Armenise, P. Favia, F. Baruzzi, K. Unger, A. Perrotta, A. M. Coclite, *Pharmaceutics* **2020**, *12*, 213.
[51] M. Krauter, M. Tazreiter, A. Perrotta, A. M. Coclite, *Macromolecules* **2020**, *53*, 7962.
[52] P. Karandikar, M. Gupta, *Thin Solid Films* **2017**, *635*, 17.
[53] A. M. Coclite, *Surf. Innovations* **2013**, *1*, 6.
[54] K. Unger, R. Resel, A. M. Coclite, *Macromol. Chem. Phys.* **2016**, *217*, 2372.
[55] A. Buchberger, S. Peterka, A. M. Coclite, A. Bergmann, *Sensors* **2019**, *19*, 999.
[56] O. Werzer, S. Tumphart, R. Keimel, P. Christian, A. M. Coclite, *Soft Matter* **2019**, *15*, 1853.
[57] F. Muralter, A. Perrotta, A. M. Coclite, *Proceedings* **2018**, *2*, 757.
[58] K. Unger, P. Salzmann, C. Masciullo, M. Cecchini, G. Koller, A. M. Coclite, *ACS Appl. Mater. Interfaces* **2017**, *9*, 17408.
[59] C. D. Petruczok, E. Armagan, G. O. Ince, K. K. Gleason, *Macromol. Rapid Commun.* **2014**, *35*, 1345.
[60] S. Sayin, A. Tufani, M. Emanet, G. G. Genchi, O. Sen, S. Shemshad, E. Ozdemir, G. Ciofani, G. Ozaydin Ince, *Front. Bioeng. Biotechnol.* **2019**, *7*, 309.
[61] A. Tufani, G. Ozaydin Ince, *J. Memb. Sci.* **2017**, *537*, 255.
[62] K. K. S. Lau, K. K. Gleason, *Thin Solid Films* **2008**, *516*, 678.
[63] Y. Zhao, Y. W. Luo, B. G. Li, S. Zhu, *Langmuir* **2011**, *27*, 11306.
[64] C. Ranacher, R. Resel, P. Moni, B. Cermenek, V. Hacker, A. M. Coclite, *Macromolecules* **2015**, *48*, 6177.